The Astrophysical Journal, 831:51 (9pp), 2016 November 1 doi:10.3847/0004-637X/831/1/51

HIGH-ENERGY ELECTRON IRRADIATION OF INTERSTELLAR CARBONACEOUS DUST ANALOGS: COSMIC-RAY EFFECTS ON THE CARRIERS OF THE 3.4 μm ABSORPTION BAND

Belén Maté, Germán Molpeceres, Miguel Jiménez-Redondo, Isabel Tanarro, and Víctor J. Herrero
Instituto de Estructura de la Materia, IEM-CSIC, Serrano 123, E-28006 Madrid, Spain
Received 2016 June 17; revised 2016 August 10; accepted 2016 August 10; published 2016 October 26

ABSTRACT

The effects of cosmic rays on the carriers of the interstellar 3.4 μm absorption band have been investigated in the laboratory. This band is attributed to stretching vibrations of CH_3 and CH_2 in carbonaceous dust. It is widely observed in the diffuse interstellar medium, but disappears in dense clouds. Destruction of CH_3 and CH_2 by cosmic rays could become relevant in dense clouds, shielded from the external ultraviolet field. For the simulations, samples of hydrogenated amorphous carbon (a-C:H) have been irradiated with 5 keV electrons. The decay of the band intensity versus electron fluence reflects a-C:H dehydrogenation, which is well described by a model assuming that H_2 molecules, formed by the recombination of H atoms liberated through CH bond breaking, diffuse out of the sample. The CH bond destruction rates derived from the present experiments are in good accordance with those from previous ion irradiation experiments of HAC. The experimental simplicity of electron bombardment has allowed the use of higher-energy doses than in the ion experiments. The effects of cosmic rays on the aliphatic components of cosmic dust are found to be small. The estimated cosmic-ray destruction times for the 3.4 μm band carriers lie in the 10^8 yr range and cannot account for the disappearance of this band in dense clouds, which have characteristic lifetimes of 3×10^7 yr. The results invite a more detailed investigation of the mechanisms of CH bond formation and breaking in the intermediate region between diffuse and dense clouds.

Key words: astrochemistry – dust, extinction – infrared: ISM – methods: laboratory: molecular – techniques: spectroscopic

1. INTRODUCTION

The 3.4 μm IR absorption band, which is widely observed in the diffuse interstellar medium (DIM) and has also been found in extragalactic sources (Wickramasinghe & Allen 1980; Duley & Williams 1983; Adamson et al. 1990; Sandford et al. 1991; Pendleton et al. 1994; Whittet et al. 1997; Imanishi 2000; Chiar et al. 2002; Mason et al. 2004; Kondo et al. 2012, and references in these articles), is associated with the presence of carbonaceous interstellar (IS) dust. The band is mostly assigned to CH stretching vibrations of CH_2 and CH_3 aliphatic groups and is related to weaker absorptions at 6.8 and 7.7 μm corresponding to bending motions of the same functional groups. Estimates about the amount of elemental carbon locked up in interstellar dust range from 5% to 30% (Sandford et al. 1991; Duley 1994; Duley et al. 1998; Furton et al. 1999). This imprecise range reflects the uncertainty about the nature of the likely carbon carriers and, consequently, about the band strengths of the IR absorption. In dense, molecular clouds, the 3.4 μm band is not observed.

Candidates for the carriers of the 3.4 μm band have been fabricated in laboratories using various procedures, including laser ablation or pyrolysis of carbon-containing precursors (Mennella et al. 1999; Schnaiter et al. 1999; Duley et al. 2005; Jäger et al. 2008), plasma deposition (Furton et al. 1999; Kovacevic et al. 2005; Godard et al. 2011; Maté et al. 2014), combustion (Pino et al. 2008), or low-temperature photolysis of hydrocarbons (Dartois et al. 2004, 2005). A thorough discussion on the suitability of the various types of laboratory candidates can be found in Pendleton & Allamandolla (2002). All the laboratory analogs of IS carbon dust have disordered structures with variable mixtures of aromatic and aliphatic groups. Among them, hydrogenated amorphous carbon (abbreviated a-C:H or HAC) leads to the best agreement with the observations.

The formation and destruction of the aliphatic structures responsible for the interstellar 3.4 μm band have been attributed to the interaction of carbonaceous solids, generated in the shells of evolved stars, with hydrogen atoms, UV photons, and cosmic rays (CRs; Chiar et al. 2013; Jones et al. 2013). UV photons and CRs lead to dehydrogenation and graphitization of dust analogs (Mennella et al. 2001, 2003; Gadallah et al. 2012; Godard et al. 2011; Alata et al. 2014), whereas interaction with H atoms has been found to reconstruct aliphatic structures (Mennella et al. 2002). In the DIM, the effects of the intense UV field prevail over those of CRs, but in denser regions, shrouded from UV radiation, CRs can become relevant.

The effects of CRs on carbonaceous dust analogs have been investigated by Mennella et al. (2003) and by Godard et al. (2011). In the first of these studies, 30 keV He^+ ions were used to simulate CRs, and analogs of IS carbonaceous dust were prepared by establishing an arc discharge between graphite electrodes in a hydrogen atmosphere, and by hydrogenation of laser-ablated carbon grains with a flow of H atoms from a microwave discharge. The authors used the approximation of monoenergetic protons for the estimation of CR effects from their He^+ data. In the investigation of Godard et al. (2011), samples of soot and of plasma-deposited a-C:H were taken as dust analogs and bombarded with a variety of high-energy ions ranging from protons to Ni^{9+}. The authors considered CR ion distributions from the literature and used a model of H-atom recombination within the irradiated samples for the treatment of their data. The estimated CR destruction rates of the 3.4 μm band derived by the two groups differ by an order of magnitude. The difference is relevant since with the destruction rate of Mennella et al. (2003), CRs might play some role in the

destruction of the aliphatic carriers of the 3.4 μm band in the interior of dense clouds, whereas with that of Godard et al. (2011) the destruction would be much slower and would be irrelevant over the entire lifetime of the clouds.

In recent works, the possibility of using high-energy (keV) electrons to mimic the effects of CRs on matter has been emphasized (Kaiser et al. 2013; Mason et al. 2014). Electron irradiation cannot certainly substitute the more rigorous experiments on bombardment with specific ions, but can provide valuable data on the global effect of CRs. The rationale behind this assertion lies in the fact that the chemical effects of CRs are not directly due to the impinging high-energy particles, but to secondary electrons and bremsstrahlung photons of much lower energy (a few eV to tens of eV) that are much more efficient for bond breaking. To a first approximation, the effects of high-energy particle processing depend on the energy dose taken by the sample rather than on the specific processing agent. In this respect, electrons in the keV range turn out to be very useful since their energy transfer per unit sample length is similar to that of MeV protons (Kaiser et al. 2013), which are often used for laboratory simulations of the effect of CRs. The adequacy of electron bombardment for the simulation of CR effects was corroborated in a recent investigation by our group (Maté et al. 2015), where glycine lifetimes, estimated for various astronomical environments from electron irradiation data, were found to be in good agreement with those from the ion irradiation experiments of Gerakines et al. (2012) carried out with 0.8 MeV protons.

In a previous work by our group we observed the effects of 2 keV electrons on a-C:H samples (Maté et al. 2014). However, no quantitative information on a-C:H destruction by electrons could be derived from these experiments carried out with too high electron fluxes and thick deposits. In the present study, which supersedes our older measurements, we address the effects of 5 keV electrons on the 3.4 μm band of a-C:H deposits generated in cold plasmas. Changes in the band profile and the decay of the total band intensity are recorded as a function of electron fluence. Total destruction cross sections are derived from our measurements at 300 and at 85 K. The results are compared with the previous investigations of Mennella et al. (2003) and Godard et al. (2011) on the bombardment of dust analogs by high-energy ions, and implications for the destruction rate of the carriers of the 3.4 μm band by CRs in the interstellar medium are discussed.

2. EXPERIMENTAL

Deposits of a-C:H were generated on IR transparent Si substrates in an inductively coupled radiofrequency (RF) plasma (Maté et al. 2014). Mixtures of CH_4 and He were used as plasma precursors. The Si substrates with the a-C:H deposits were then taken to the sample compartment of a Fourier transform infrared (FTIR) spectrometer, where spectra of the 3.4 μm band were recorded for control and thickness measurement. For a given set of deposition conditions, the band shape and intensity were very repetitive and the integrated absorbance was proportional to the deposition time. IR interference fringes could be used to estimate the width of samples thicker than $\approx$800 nm. For thinner samples, the width was extrapolated using the deposition time. An uncertainty of $\pm$30 nm is estimated in the width values. For the processing experiments of this work, four a-C:H samples, S1 (520 nm), S2 (540 nm), S3 (490 nm), and S4 (420 nm), were used. This thickness range was chosen to maximize the spectral intensities while guaranteeing electron irradiation of the whole sample (see below). For the generation of these deposits, flows of methane and He of 5 and 10 sccm, respectively, were allowed into the reactor. The total pressure before plasma ignition was 0.32 mbar, and the discharge power was 40 W. The deposition time was $\approx$15 minutes. In the time between experiments, the deposits were kept in a sealed box under inert gas pressure to minimize oxidation.

The a-C:H deposits were then transferred to a high-vacuum chamber for processing (see Maté et al. 2014 for details of the setup). The Si substrates with the deposits were placed in an appropriate Cu holder in contact with a liquid nitrogen Dewar, mounted in a rotatable flange. During processing, the substrates were made to face alternatively the IR beam from an FTIR spectrometer or the electron beam from an electron gun inside the chamber. The samples were irradiated with a 7.9×10^{12} electron cm^{-2} s^{-1} homogeneous flux of 5 keV electrons at normal incidence. At given intervals, electron irradiation was interrupted and the sample was rotated to record IR transmission spectra at normal incidence. Typical irradiation times of 350 minutes (electron fluences 1.7×10^{17} electrons cm^{-2}) were used. The experiments were carried out for sample temperatures of 85 (S1 and S3) and 300 K (S2 and S4).

The penetration depth of the 5 keV electrons in the a-C:H samples was estimated by means of Monte Carlo simulations using the CASINO (monte CArlo SImulations of electroN trajectories in sOlids) code (Drouin et al. 2007; Drouin 2011). Although the composition (H/C ratio) and densities of the a-C:H deposits are not known with precision, we have assumed a density of 1.2 g cm^{-3} and an H/C ratio of 1 in analogy with Godard et al. (2011), who used also RF discharges of methane for the generation of their samples. These values are also consistent with the results of other authors for similar methane plasmas (Schwarz-Selinger et al. 1999). A comparison with literature work on plasma-generated a-C:H samples (see, e.g., Angus & Jensen 1988; Robertson 1996; Godard & Dartois 2010, and references cited therein) suggests that the fraction of sp^2 C atoms in our deposits, defined as $sp^2/(sp^2 + sp^3)$, should be in the $\approx$0.20–0.40 range. The penetration depth calculated with CASINO is $\approx$530 nm. Variations in the estimated penetration depths are small for densities in the 1–1.5 g cm^{-3} range and for C/H ratios between 0.5 and 1.

3. RESULTS AND DISCUSSION

The upper panels of Figure 1 show the 3.4 μm band of the S1 and S2 deposits before irradiation. Three peaks stand out in the characteristic band contour. A conventional decomposition of the band into the stretching modes of CH, CH_2, and CH_3 groups using adjustable Gaussian functions (see, e.g., Sandford et al. 1991; Dartois et al. 2004; Duley et al. 2005; Dartois et al. 2007; Chiar et al. 2013) is also shown. According to this decomposition, the two higher peaks of the band, in order of decreasing frequency, correspond largely to antisymmetric CH stretching vibrations of CH_3 and CH_2, respectively, and the third peak contains the unresolved contributions of the corresponding symmetric modes. Aromatic or olefinic CH stretching is assumed to be responsible for the wing at higher frequencies. This non-aliphatic component makes up about 10% of the band intensity. Some authors suggest also small contributions from a Fermi resonance with bending modes

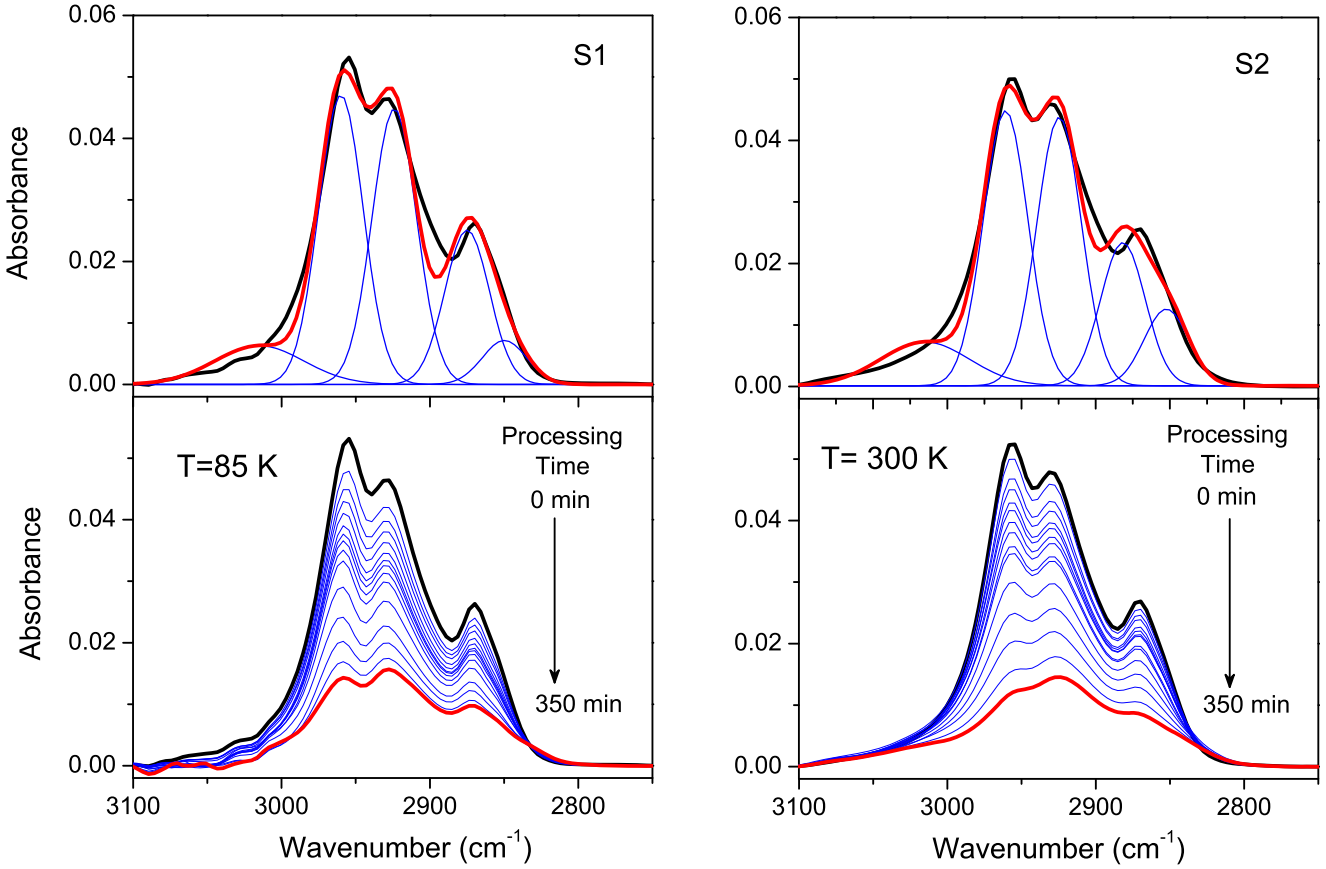

Figure 1. Upper panels: decomposition of the 3.4 μm band of samples S1 and S2 into a sum of five Gaussians. Black trace: observed spectrum. Red trace: sum of proposed five components. Lower panels: evolution of the band, as a function of time, under 5 keV electron irradiation at 85 and 300 K.

Table 1
Band Decomposition of the Unprocessed a-C:H Deposits for the Four Samples (S1–S4) Used

	S1 (520 nm)			S2 (540 nm)			S3 (490 nm)			S4 (420 nm)		
Stretch Mode	P cm^{-1}	W cm^{-1}	A cm^{-1}	P cm^{-1}	W cm^{-1}	A cm^{-1}	P cm^{-1}	W cm^{-1}	A cm^{-1}	P cm^{-1}	W cm^{-1}	A cm^{-1}
CH arom	3010	60	0.51	3008	60	0.55	3010	60	0.60	3010	60	0.50
CH_3 asym	2959	30	1.83	2959	30	1.81	2960	30	1.85	2959	30	1.75
CH_2 asym	2921	30	1.63	2922	30	1.70	2922	30	1.57	2922	30	1.57
CH_3 sym	2876	30	0.86	2876	30	0.94	2875	30	0.75	2877	30	0.83
CH_2 sym	2851	30	0.35	2851	30	0.33	2845	30	0.45	2853	30	0.34

Note. P, W, and A indicate the peak position, the width of the fitted Gaussian, and the integrated area of each band, respectively.

(Dartois et al. 2007) or from CH modes of tertiary carbons (Allamandola et al. 1992), but we have not considered them here. The peak positions, widths, and areas of the Gaussians in the band profile decomposition of the four a-C:H samples studied are listed in Table 1.

The lower panels of Figure 1 display the evolution of the band intensity and profile of the a-C:H deposit under electron bombardment at 85 and 300 K. At the end of the experiments, after 350 minutes of irradiation by 5 keV electrons, the overall band intensity decreases markedly, and the band contour is appreciably modified. In the unprocessed a-C:H samples the maximum of the band corresponds to the high-frequency peak, but this peak decreases faster than the other two, and at the end of the processing experiments the middle peak dominates the band profile.

Assuming the band decomposition shown in the upper panels of Figure 1 and in Table 1, one can take the time evolution of the areas under the Gaussians of the two highest peaks, which are assigned to the asymmetric stretch vibrations of CH_3 and CH_2 groups, respectively, as a measure of the relative stability of these groups against electron bombardment.

This evolution is shown in Figure 2. The corresponding symmetric stretch contributions are not adequate to this aim since they are blended in the third peak and the decomposition is much less reliable and has not been used. As can be seen, the CH_3 curve decreases faster than that of CH_2, indicating that methyl groups in the initial a-C:H structure are more easily destroyed by electron bombardment than methylene groups. This behavior is in accordance with intuitive expectations, since statistically the probability of CH bond breaking is higher in methyl, with three CH bonds, than in methylene, with just two. Moreover, breaking of one of the CH_3 bonds will often lead to the formation of a CH_2 group. It should be stressed that the vibrational mode assignment reflected in Figure 1 and

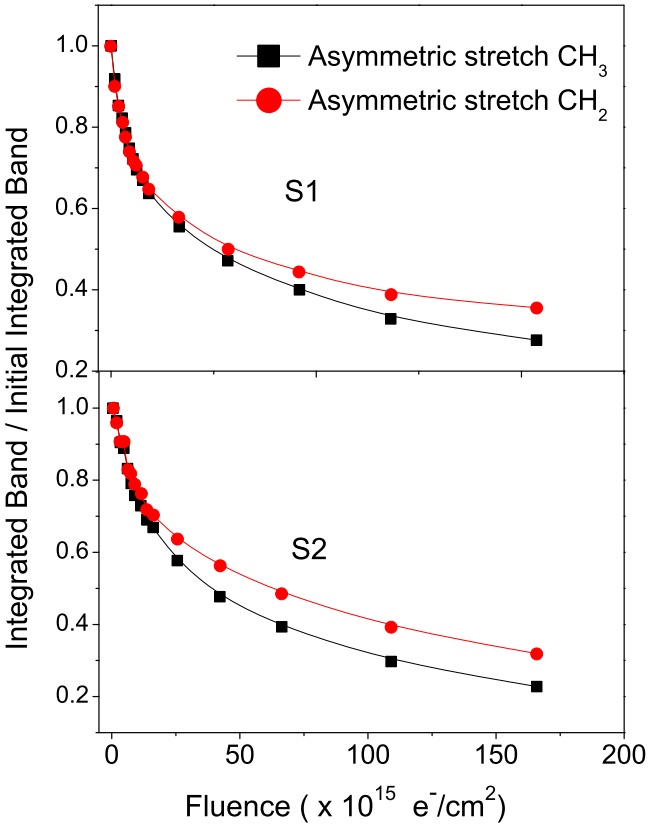

Figure 2. Evolution of the relative intensities of the CH_3 and CH_2 asymmetric stretching peaks with electron fluence. Upper panel: S1 sample, irradiated at 85 K; lower panel: S2 sample, irradiated at 300 K.

Table 2
Parameters from the H-atom Recombination Model (Equation (2)) for the Electron Irradiation Experiments and Recombination Volume

Sample Temperature (K)	$\sigma_d^r(\times 10^{17})$ cm^2	I_f/I_0	V (Å^3)
85	1.0 ± 0.2	0.21 ± 0.02	85
300	1.2 ± 0.2	0.28 ± 0.02	64

Table 2 is only an approximation and that a significant degree of mode mixing is expected for the complex structure of a-C:H. From now on, we will consider just the evolution of the integrated band intensity and will not elaborate on the specific functional group of the CH bonds.

Figure 3 shows the decrease in the relative intensity of the 3.4 μm band as a function of electron fluence for the four a-C:H samples investigated. The intensity drop is comparatively steep at the beginning and becomes more gradual for larger irradiation fluences. A similar trend was observed in the ion irradiation experiments of Mennella et al. (2003) and Godard et al. (2011) and was attributed to dehydrogenation. A model to account for the hydrogen release induced by ion irradiation of a-C:H was advanced by Adel et al. (1989) and Marée et al. (1996). The model assumes that hydrogen leaves a-C:H in molecular form. When a CH bond is broken, the hydrogen atom diffuses within the solid, where it can recombine with another H atom to produce H_2, or be trapped by a reactive site in the bulk material. Once formed, the H_2 molecules are stable and diffuse out of the solid. Under continued irradiation, the H-atom density drops to a point where recombination stops, when

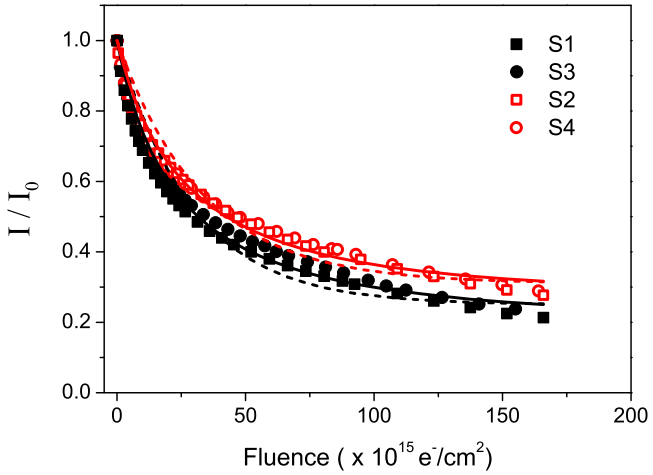

Figure 3. Decay of the 3.4 μm band intensity under 5 keV electron bombardment. Black filled symbols: samples processed at 85 K (squares: S1 [520 nm]; circles: S3 [490 nm]). Red open symbols: samples processed at 300 K (squares: S2 [540 nm]; circles: S4 [420 nm]). Solid curves: fits to the data with the recombination model of Equation (2). Dashed curves: exponential fits to the data (Equation (3)).

H atoms from broken CH bonds react at a solid active site before finding another H atom.

In the formulation of Adel et al. (1989) the evolution of H-atom density with ion fluence can be expressed as

$$n_{\rm H}(F) = \left[\frac{1}{n_{\rm Hf}} + \left(\frac{1}{n_{\rm H0}} - \frac{1}{n_{\rm Hf}}\right)\exp(-\sigma_{\rm d}^{r}F)\right]^{-1}, \qquad (1)$$

where $n_{\rm H}$ is the H-atom density, F the ion fluence, $n_{\rm H0}$ the initial H-atom density, $n_{\rm Hf}$ the asymptotic H-atom density for infinite fluence, and $\sigma_{\rm d}^{\rm r}$ an effective dehydrogenation cross section for the recombination model. Assuming that the absorption intensity of the 3.4 μm band is proportional to the hydrogen-atom density (Godard et al. 2011), Equation (1) can be rewritten as

$$\frac{I(F)}{I_0} = \left[\frac{I_0}{I_f} + \left(1 - \frac{I_0}{I_f}\right)\exp(-\sigma_{\rm d}^{r}F)\right]^{-1}, \qquad (2)$$

where $I(F)$ is the integrated band intensity for a fluence F, I_0 the initial band intensity, and $I_{\rm f}$ the asymptotic final intensity. Equation (2) provides a good description of the experimental results of Godard et al. (2011) on the irradiation of a-C:H and soot samples with different high-energy ions. From a fit of this equation to their measurements, the authors derived destruction cross sections for the band carriers (CH bonds).

In accordance with previous publications (Kaiser et al. 2013; Mason et al. 2014; Maté et al. 2015), we have assumed that the effects of high-energy electrons are comparable to those of high-energy ions if the sample width does not exceed appreciably the electron penetration depth, and we have also adopted the hydrogen-atom recombination model (Adel et al. 1989; Marée et al. 1996) to evaluate our measurements and have adjusted the experimental decay data to Equation (2). In our experiments, the intensity decrease is somewhat more pronounced for the samples irradiated at 85 K than for those irradiated at 300 K. We have fitted the joint irradiation data from S1 and S3 for 85 K and the joint irradiation data from S2

Table 3
Parameters of the Exponential Fit (Equation (3))
for the Electron Irradiation Experiments

Sample Temperature (K)	σ_d^e ($\times 10^{17}$) cm^2	I_f/I_0	V (Å^3)
85	3.4 ± 0.2	0.25 ± 0.02	71
300	3.0 ± 0.2	0.31 ± 0.02	57

and S4 for 300 K. The resulting curves, which are displayed in Figure 3, provide a reasonably good description of the band decay over the whole fluence range investigated. The destruction cross sections, σ_d^r, and the asymptotic relative band intensities (I_0/I_f) are given in Table 2.

The differences between the parameters for two temperatures are not large and, in the case of the cross sections, lie within the mutual uncertainty. In the spirit of the recombination model, the higher asymptotic band intensity obtained for 300 K would mean that the balance between H_2 formation and trapping of H atoms by a reactive site of the solid shifts toward the latter for the higher temperature. In any case, the temperature dependence is weak.

The asymptotic H-atom density, n_{Hf}, in Equation (1) defines a characteristic recombination volume ($V = 1/n_{Hf}$) within the solid. When the density drops to n_{Hf}, free H atoms released by electron irradiation are too far apart and get trapped by the solid before recombining to form H_2. Although the precise density and H proportion of the deposited a-C:H samples are not accurately known, we can make reasonable assumptions to estimate V values. As indicated above, we have taken a density of 1.2 g cm^{-3} and a hydrogen-atom ratio H/C = 1 for our plasma-deposited a-C:H, in analogy with Godard et al. (2011). The corresponding H-atom density is $n_{H0} = 5.6 \times 10^{22}$ cm^{-3}. The destruction cross sections from Table 2 are lower than those obtained by Godard et al. (2011) for a-C:H bombardment with ions using the same fit model. In the case of 10 MeV protons the difference is less than a factor of two, but it is typically more than an order of magnitude larger for heavier and multicharged ions. Recombination volumes of tens of Å^3, like those derived from our fits, are also typical for the ion irradiation experiments.

The evolution of the 3.4 μm band observed in the irradiation experiments of Mennella et al. (2003) with 30 keV He^+ ions was satisfactorily fitted by an exponential decay, with a phenomenological destruction cross section, plus an added constant accounting for the asymptotic H concentration. In terms of the band intensity, this behavior can be expressed as

$$\frac{I(F)}{I_0} = a\ \exp(-\sigma_d^e F) + \frac{I_f}{I_0}, \quad (3)$$

where σ_d^e is a destruction cross section for the exponential decay, α is a fitting constant, and the meaning of the rest of the symbols is the same as in Equations (1) and (2). In this equation, the reformation of CH bonds is implicitly assumed by the existence of a nonzero asymptotic value for I_f, but, in contrast to the recombination model, no hypothesis about the specific mechanism of dehydrogenation is considered. The exponential decay of Equation (3) leads to similar asymptotic band intensities, but to larger cross sections than the recombination model (see Table 3); it provides also a worse global fit to the measurements (see Figure 3).

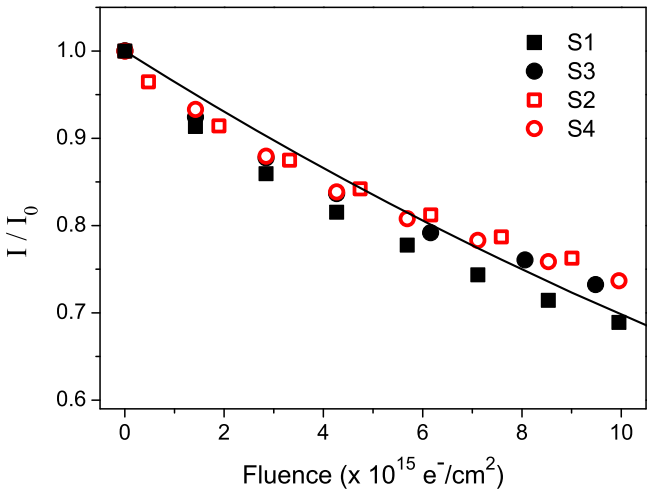

Figure 4. Fits of the 3.4 μm band decay with an exponential function (Equation (4)) for electron fluences lower than 1×10^{16} cm^{-2}. Symbols are the same as in Figure 3. Solid line: fit using Equation (4).

Godard et al. (2011) verified also that an exponential fit (Equation (3)) to their ion irradiation data led to a worse agreement with the measurements and to higher values of the fitted cross sections than those obtained with the recombination model. It should be noted at this point that both the H-atom recombination model and even more so the phenomenological exponential decay provide only simple approximate descriptions of the actual processes. A more realistic view should take into account that a simple destruction cross section might not be enough to account for energetic processing leading to a gradual transformation of the material and that stable chemical species other than H_2, such as CH_4 or other hydrocarbons, might also evolve and contribute to the decay of the 3.4 μm band (Alata et al. 2014, 2015; Duley et al. 2015; Jones & Habart 2015).

At the beginning of the irradiation process (electron fluences lower than $\approx 10^{16}$ cm^{-2}), the band decay for all data is reasonably well accounted for by a simple exponential function, tending asymptotically to zero:

$$\frac{I(F)}{I_0} = \exp(-\sigma_d^e F). \quad (4)$$

The fit of Equation (4) to our data is displayed in Figure 4.

A σ_d^e value of $(3.6 \pm 0.1) \times 10^{-17}$ cm^{-2} can account approximately for the low-fluency decay at the two temperatures. It provides an approximate upper limit to the destruction cross section of the a-C:H deposits by 5 keV electrons.

To perform a direct comparison of the effects of our 5 keV electron bombardment on a-C:H with those of high-energy ion irradiation of Godard et al. (2011), we have represented in Figure 5 the evolution of the 3.4 μm band as a function of the energy deposited per unit mass sample, $\Delta E(F)$, which can be calculated as

$$\Delta E(F) = \text{LET} \times F \times \rho_{HAC}^{-1}, \quad (5)$$

where LET is the linear energy transfer of the bombarding electrons, F the electron fluence, and $\rho_{a\text{-}C:H}$ the a-C:H density. As indicated in Section 2, a penetration depth of $\approx$530 nm is obtained with the CASINO Monte Carlo simulation (Drouin et al. 2007; Drouin 2011) for the assumed values of a-C:H

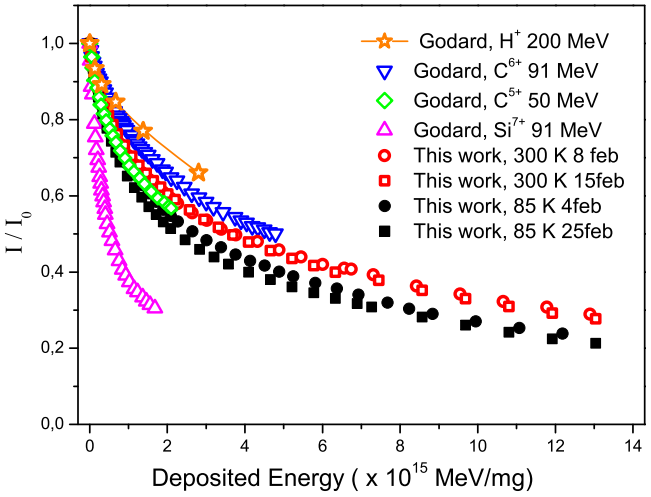

Figure 5. Comparison of the effects of ion (Godard et al. 2011) and electron (present experiments) irradiation on a-C:H samples.

density ($\rho_{\text{a-C:H}} = 1.2\,\text{g cm}^{-3}$) and hydrogen proportion (H/C = 1), which corresponds to an LET of $9.4\,\text{eV nm}^{-1}$. We have taken this value of the LET in all cases, since CASINO simulations further show that the LET hardly varies over the range of thickness values of our samples (420–540 nm).

For clarity of display, only a few ions are represented in the figure to delimit the range of destruction efficiencies; the reader is referred to Figure 3 of Godard et al. (2011) for the original data on the whole ion set. The efficiency of 5 keV electrons for the destruction of the carriers of the 3.4 μm band is found to be somewhat higher than that of protons, comparable to that of carbon ions and lower than that of heavy ions. The energy doses sampled in the present electron bombardment experiments are appreciably larger than those of the previous ion bombardment measurements. It is reassuring that even for this extended range, the simple H-atom recombination model can account reasonably well for the observed behavior (see Figure 3). The validity of this approximate method, which uses a single destruction cross section irrespective of the possible structural modifications of the bombarded material, is strengthened by results of the ion irradiation experiments of Godard et al. (2011) on soot samples with a higher density ($1.8\,\text{g cm}^{-3}$) and a much smaller hydrogen content (H/C = 0.01) than a-C:H. The latter results yielded comparable CH destruction efficiencies showing that the destruction cross section of CH bonds for a given energetic ion is only weakly dependent on the carbonaceous material.

4. ASTROPHYSICAL IMPLICATIONS

We adopt the monoenergetic proton approximation (Strazzulla & Johnson 1991; Moore et al. 2001, and references therein) to estimate the destruction rate of CH bonds in diffuse clouds from our electron bombardment measurements. This approximation was also applied by Mennella et al. (2003) for the evaluation of their measurements on a-C:H irradiation with 30 keV He^+ ions, and here we follow closely their formulation. Within this approximation, the CR destruction rate, $R_{\text{d,CR}}$, is expressed as

$$R_{\text{d,CR}} \approx \sigma_{\text{d,p}}(1\ \text{MeV})\,\phi_{\text{p}}(1\ \text{MeV}), \quad (6)$$

Table 4
Cosmic-ray CH Bond Destruction Rates, $R_{\text{d,CR}}$, in the Diffuse ISM Estimated from Our Measurements Using the 1 MeV Monoenergetic Proton Approximation (see the text and Mennella et al. 2003)

C Dust Temperature (K)	$R_{\text{d CR}}$ (s^{-1}) Recombination Model	$R_{\text{d CR}}$ (s^{-1}) Exponential Fit
85	7.0×10^{-17}	2.0×10^{-16}
300	5.9×10^{-17}	1.8×10^{-16}

Table 5
Comparison of Cosmic-ray CH Destruction Rates in the Diffuse ISM Estimated from Electron and Ion Bombardment Data

Source	Destruction Rate, $R_{\text{d CR}}(\text{s}^{-1})$
Present work (average of 85 and 300 K)	6.6×10^{-17} (rec. model); 1.9×10^{-16} (exp. fit)
Mennella et al. (2003)	1.7×10^{-15}
Godard et al. (2011)	3.0×10^{-17}–3.3×10^{-16}

where $\sigma_{\text{d,p}}$ (1 MeV) is the destruction cross section by 1 MeV protons and ϕ_{p} is an effective quantity that represents the flux of 1 MeV protons that would lead to the same ionization as the whole CR distribution. $\phi_{\text{p}}(1\,\text{MeV})$ can be estimated from models giving the CR ionization rate, ζ_{CR}, and the ionization cross section for 1 MeV protons in different environments. In analogy with Mennella et al. (2003), we take here a value $\phi_{\text{p}}(1\,\text{MeV})$ of 1.8 and $1\,\text{cm}^{-2}\,\text{s}^{-1}$ for diffuse and dense clouds, respectively, which are based on a ζ_{CR} value of $6 \times 10^{-17}\,\text{s}^{-1}$ and on ionization estimates by Spitzer & Tomashko (1968) and Cravens & Dalgarno (1978). For the evaluation of $\sigma_{\text{d,p}}$ (1 MeV) we use our σ_{d} values for 5 keV electrons and assume, also in analogy with Mennella et al. (2003), that the destruction cross section is directly proportional to the stopping cross section, S, of a-C:H for a given particle. We can now write

$$\sigma_{\text{d,p}}(1\ \text{MeV}) = \frac{S_{\text{p}}(1\ \text{MeV})}{S_{e}(5\ \text{keV})}\sigma_{\text{d,e}}(5\ \text{keV}). \quad (7)$$

The stopping cross section of a-C:H for our 5 keV electrons is $S_{\text{e}}\,(5\,\text{keV}) = \text{LET} \times \rho_{\text{a-C:H}}^{-1} = 7.9 \times 10^{-2}\,\text{MeV mg}^{-1}\,\text{cm}^2$ and that for 1 MeV protons is $S_{\text{p}}\,(1\,\text{MeV}) = 2.62 \times 10^{-1}\,\text{MeV mg}^{-1}\,\text{cm}^2$ as calculated with the Stopping and Range of Ions in Matter (SRIM) code (Ziegler et al. 2010) for our assumed a-C:H composition (C/H = 1) . Mennella et al. (2003) used a very similar value ($2.60 \times 10^{-1}\,\text{MeV mg}^{-1}\,\text{cm}^2$) for the evaluation of their data. Substituting these stopping cross sections in Equation (7) and using the $\sigma_{\text{d,e}}$ values from our experiments, we obtain the CR dissociation rates listed in Table 4.

The CR destruction rates derived from our measurements are compared in Table 5 with those from the ion irradiation experiments of Mennella et al. (2003) and Godard et al. (2011). The value of Mennella et al. (2003) was derived with the same monoenenrgetic proton approximation used in the present work. Godard et al. (2011) took advantage of their measurements with multiple ions and used a more elaborated method considering explicitly the distribution of elements in CRs. They assumed also that the dependence of the destruction cross section, σ_{d}, on the stopping cross section, S, could take the form $\sigma_{\text{d}} = K\,S^{\alpha}$, with K a proportionality constant and α between 1 and 1.4, and considered different models for the CR

ionization rate ζ_{CR}. In Table 5 we indicate also the interval of CH destruction rate values reported by these authors.

As can be seen, the destruction rates from the present work are comparable to those of Godard et al. (2011) and one order of magnitude lower than that of Mennella et al. (2003). The good agreement with the thorough work of Godard et al. (2011) is reassuring and confirms once more the adequacy of using high-energy electrons for the investigation of CR effects on interstellar particles, at least to a first approximation. Electron bombardment experiments also have limitations. They do not inform on the specific role of heavy CR elements like Fe ions, which might play some role in the long-term destruction of CH bonds, and they do not allow the simulation of the effects of the element distribution in CRs (Godard et al. 2011). On the other hand, electron bombardment measurements are experimentally simple and offer the possibility of depositing higher-energy doses in the carbonaceous dust analogs, which is tantamount to exploring the effects of CRs over a longer time.

The reasons for the discrepancy of the present results and those of Godard et al. (2011) with the value of Mennella et al. (2003) are not clear. Different CR models were used by Godard et al. (2011) for the derivation of their destruction rates, but in the present work we have applied exactly the same approximation as Mennella et al. (2003) for the CR flow. A significant difference between the work of Mennella et al. (2003) and the other two lies in the procedure of generation of the dust analogs. Plasma-generated a-C:H deposits were taken as irradiation targets in this work and also in the experiments of Godard et al. (2011), whereas in the measurements of Mennella et al. (2003) an arch discharge or laser ablation techniques were applied for the production of the analogs. However, this difference in the nature of the dust analogs does not seem likely to justify the large discrepancy in the destruction rates, since, as mentioned above, the comparison of ion irradiation experiments on very different soot and a-C:H samples (Godard et al. 2011) points just to a weak dependence of the CH bond destruction on the specific carbonaceous material.

Characteristic times for the CR destruction of CH bonds can be roughly estimated as the inverse of the destruction rates, $\tau_{d,CR} = R_{d,CR}^{-1}$. In Table 6 these characteristic times are compared with the times for UV bond destruction or to bond formation through interaction with H atoms in typical diffuse and dense interstellar regions.

The formation of CH bonds, and specifically of aliphatic structures, which would be mostly responsible for the presence of the 3.4 μm band, is assumed to take place in the DIM through the interaction of H atoms with hydrogen-poor carbon grains formed in the envelopes of evolved stars. In this environment the rates of bond formation and of destruction by UV photons are relatively high, but the balance is shifted toward hydrogenation. This view is consistent with the characteristic times for CH formation and destruction derived from the experiments of Mennella et al. (2001, 2002), shown in Table 6. In this environment, the intense UV field is dominant and CRs would play a negligible role in the overall destruction of CH bonds, in spite of the fact that their destruction cross sections are orders of magnitude larger than those of UV photons.

The disappearance of the 3.4 μm band in dense clouds is not so well understood. The interior of dense clouds is shielded from the galactic UV field, and although the UV flux drops sharply, the actual penetration of these photons into the clouds is not known with precision, since it depends strongly on grain properties (Roberge et al. 1991). The proportion of H atoms in the gas phase drops also rapidly with growing extinction (A_V) as most of them recombine to form H_2 molecules (see, e.g., Le Petit et al. 2006). Experimental evidence also indicates that ice mantles are formed on grains beyond $A_V = 3$ (Whittet et al. 2001), and depending on their width, these mantles protect, at least partially, the grain surface from hydrogenation and from UV processing. With the decrease of the influence of H atoms and UV photons, the role of CRs, whose flux does not change much inside dense clouds, becomes more important. Characteristic CR destruction times estimated from the experiments of Mennella et al. (2003) are of the order of the cloud lifetime (10^7 yr) and could in principle lead to an appreciable destruction of CH bonds in hydrocarbon dust, but the results of the present work, which corroborate the previous values of Godard el al. (2011), indicate that the direct effects of CRs on the carriers of the 3.4 μm should be negligible over the whole lifetime of a typical molecular cloud. Alternative mechanisms must be invoked to justify the observations.

CRs have an important indirect effect in dense clouds, namely, the production of a secondary UV field through the excitation of H_2 fluorescent levels. The flux of secondary UV photons could reach 10^4 cm^{-2} s^{-1} (Prasad & Tarafdar 1983), as compared with the 8×10^7 cm^{-2} s^{-1} photon flux estimated for the galactic UV field outside the clouds (Mathis et al. 1983). The CH destruction time associated with this secondary UV field would be of the order of 10^7 yr for unshielded grain surfaces. This time is shorter by an order of magnitude than that estimated in this work and also in the study of Godard et al. (2011) for direct CH bond destruction by CRs. Nevertheless, as

Table 6
Characteristic Times for CH Bond Destruction and Formation as Compared with the Dynamical Times of Diffuse Regions and Dense Clouds

	Characteristic Time (yr)	
Parameter	Diffuse Region $A_V(\text{mag}) < 10^{-4}$	Dense Cloud $A_V(\text{mag}) > 3$
Dynamical time	$\approx 10^8$ [a]	3×10^7 [a]
CH destruction by CRs		
Present work	$(2–5) \times 10^8$	$(3–9) \times 10^8$ [b]
Godard et al. (2011)	10^8–10^9	10^8–10^9
Mennella et al. (2003)	2×10^7	3×10^7 [b]
CH destruction by UV photons		
Mennella et al. (2001)	4×10^3	$\geqslant 10^7$ [c]
CH formation by H atoms		
Mennella et al. (2002)	2×10^3	...

Notes. Typical diffuse and dense clouds conditions are indicated by the given extinction (A_V) values. The times are calculated as the inverse of the destruction rates, R_d^{-1}, and formation rates, R_f^{-1}, reported in the mentioned references.

[a] From Jones et al. (1994) and references therein. The dynamical time provides an estimate of the grain lifetime. In the diffuse medium this time is limited by shock destruction and in dense clouds by cloud collapse.

[b] Estimates in dense clouds using the monoenergetic proton approximation and assuming an effective (1 MeV) proton flux of 1 cm^2 s^{-1} as compared with 1.8 cm^2 s^{-1} in diffuse regions (Mennella et al. 2003).

[c] Based on the CR-induced UV field (10^4 photons cm^{-2} s^{-1}) of Prasad & Tarafdar (1983). The penetration of galactic UV photons is difficult to estimate, but could still be significant at $A_V = 3$ (see the text).

the grains become gradually covered with ice mantles (i.e., for $A_V > 3$), the photodestruction efficiency of the secondary UV field should decrease sharply. It is thus the region of $A_V < 3$, where the disappearance of the 3.4 μm band would be more likely. Somewhere in this region, CH bond breaking by UV photons is expected to prevail over hydrogenation and lead to the destruction of the 3.4 μm band carriers. Details of the process are at present a matter of speculation. Estimates by Chiar et al. (2013), which assume a significant penetration of the galactic UV field into the cloud, suggest that even at $A_V = 3$, galactic UV radiation would destroy the external aliphatic layer responsible for the 3.4 μm band in about 10^6 yr, before the growth of an ice mantle. A recent cosmic dust model by Jones et al. (2013, 2014), with reduced H-atom incorporation rates, suggests that photodestruction could dominate over hydrogenation down to $A_V = 0.01$, where H atoms still make a significant proportion of the gas phase.

SUMMARY AND CONCLUSIONS

The effects of CRs on the carriers of the 3.4 μm absorption band of carbonaceous dust have been investigated in the laboratory. This band is largely attributed to CH stretching vibrations of aliphatic CH_3 and CH_2 groups, with some contribution of aromatic or olefinic CH at its high-frequency wing. The a-C:H deposits generated in RF CH_4 plasmas were taken as dust analogs, and 5 keV electrons were used to mimic CR bombardment. Electron bombardment was carried out for sample temperatures of 85 and 300 K. From the decay of the band intensity as a function of electron fluence, CH destruction cross sections were derived. These cross sections, in conjunction with the monoenergetic ion approximation (Mennella et al. 2003), were used to evaluate destruction rates of CH bonds in interstellar hydrocarbon dust by CRs. The main conclusions of this work are the following:

1. Changes in the band profile during irradiation suggest that methyl groups in the a-C:H structure are destroyed more efficiently than methylene groups.
2. The decay of the 3.4 μm band as a function of electron fluence is well accounted for by a simple H recombination model, which assumes that the main dehydrogenation mechanism is the bulk formation of H_2 molecules with the H atoms liberated through CH bond breaking. The validity of the model, which was verified for ion irradiation by Godard et al. (2011), is extended here to higher-energy doses.
3. The band intensity decay tends toward a slightly larger asymptotic value at $T = 300$ K than at $T = 85$ K. This fact suggests that the balance between H recombination and H trapping at reactive solid sites is shifted toward the latter at the higher temperature. The effect is, however, small.
4. The good agreement between the CR destruction rates of the present work and those from the detailed irradiation experiments of Godard et al. (2011) involving multiple ions corroborates the adequacy of electron irradiation as a surrogate for CR interaction. The experimental simplicity and flexibility of electron bombardment measurements as compared with energetic ion irradiation allow an easy deposition of higher-energy doses in the solid samples, and thus the simulation of CR effects over a longer time. The discrepancy with the previous results by Mennella et al. (2003), which reported higher CH bond destruction rates from their 30 keV He^+ bombardment measurements, could be partly due to the different dust analogs used.
5. The CH bond destruction rates derived from the present experiments indicate that the direct effects of CRs are small and cannot account for the disappearance of the 3.4 μm band in dense clouds. The effect of the secondary UV field, induced by CRs inside dust clouds, is expected to be larger, but probably not enough to justify CH destruction, especially for ice-covered dust grains. The present results, in line with Godard et al. (2011), suggest that the destruction of the CH bonds responsible for the 3.4 μm band takes place at the transition from diffuse to molecular clouds. More work on the interaction of carbon dust with H atoms and UV photons, as well as on the modeling of the intermediate region between diffuse and dense clouds, is needed to clarify this issue.

We are indebted to R. Escribano for comments on the manuscript. This work has been funded by the MINECO of Spain under grant FIS2013-48087-C2-1P, by the MICINN of Spain under grant CDS2009-00038, and by the European project ERC-2013-Syg 610256. G.M. acknowledges MINECO PhD grant BES-2014-069355. Our skillful technicians M.A. Moreno, A. González, and J. Rodríguez are also gratefully acknowledged.

REFERENCES

Adamson, A. J., Whittet, D. C. B., & Duley, W. W. 1990, MNRAS, 243, 400
Adel, M. E., Amir, O., Kalish, R., & Feldman, L. C, R. 1989, JAP, 66, 3248
Alata, I., Cruz-Diaz, G. A., Muñoz Caro, G. M., & Dartois, E. 2014, A&A, 569, A119
Alata, I., Jallat, A., Gavilan, L., et al. 2015, A&A, 584, A123
Allamandola, L. J., Sandford, S. A., Tielens, A. G. G. M., & Herbst, T. M. 1992, ApJ, 399, 134
Angus, J. C., & Jensen, F. 1988, JVSTA, 6, 1778
Chiar, J. E., Adamson, A. J., & Pendleton, Y. J. 2002, ApJ, 570, 198
Chiar, J. E., Tielens, A. G. G. M., Adamson, A. J., & Ricca, A. 2013, ApJ, 770, 78
Cravens, T. E., & Dalgarno, A. 1978, ApJ, 219, 750
Dartois, E., Gebale, T. R., Pino, T., et al. 2007, A&A, 463, 635
Dartois, E., Muñoz Caro, G. M., Deboffle, D., & d'Hendecourt, L. 2004, A&A, 423, L33
Dartois, E., Muñoz Caro, G. M., Deboffle, D., Montagnac, G., & d'Hendecourt, L. 2005, A&A, 432, 895
Drouin, D. 2011, http://www.gel.usherbrooke.ca/casino
Drouin, D., Couture, A. R., Joly, D., et al. 2007, Scanning, 29, 92
Duley, W. W. 1994, ApJL, 430, L133
Duley, W. W., Grishko, V. I., Kenel, J., Lee-Dadswell, G., & Scott, A. 2005, ApJ, 626, 933
Duley, W. W., Scott, A. D., Seahra, D., & Dadswell, G. 1998, ApJL, 503, L183
Duley, W. W., & Williams, D. A. 1983, MNRAS, 205, 67
Duley, W. W., Zaidi, A., Wesolowski, M. J., & Kuzmin, S. 2015, MNRAS, 447, 1242
Furton, D. G., Lahio, J. W., & Witt, A. N. 1999, ApJ, 526, 752
Gadallah, K. A. K., Mutschke, H., & Jäger, C. 2012, A&A, 544, A107
Gerakines, P. A., Hudson, R. L., Moore, M. H., et al. 2012, Icar, 220, 647
Godard, M., & Dartois, E. 2010, A&A, 559, A39
Godard, M., Féraud, G., Chabot, M., et al. 2011, A&A, 529, A146
Imanishi, M. 2000, MNRAS, 319, 331
Jäger, C., Mutschke, H., Henning, Th., & Huisken, F. 2008, ApJ, 689, 249
Jones, A. P., Fanciullo, L., Köhler, M., et al. 2013, A&A, 558, A62
Jones, A. P., & Habart, E. 2015, A&A, 591, A92
Jones, A. P., Tielens, A. G. G. M., Hollenbach, D. J., & McKee, C. F. 1994, ApJ, 433, 797
Jones, A. P., Ysard, N., Köhler, M., et al. 2014, FaDi, 168, 313
Kaiser, R. I., Stockton, A. M., Kim, Y. S., Jensen, E. C., & Mathies, A. R. A. 2013, ApJ, 756, 111

Kondo, T., Kaneda, H., Oyabu, S., et al. 2012, ApJL, 751, L18
Kovacevic, E., Stefanovic, I., Berndt, J., Pendleton, Y. J., & Winter, J. 2005, ApJ, 623, 242
Le Petit, F., Nehme, C., Le Bourlot, J., & Roueff, E. 2006, ApJS, 164, 506
Marée, C. H. M., Vredenberg, A. M., & Habraken, F. H. P. M. 1996, Mat. Chem. Phys, 46, 198
Mason, N. J., Nailr, B., Jheeta, S., & Szimañska, E. 2014, FaDi, 168, 235
Mason, R. E., Wright, G., Pendleton, Y., & Adamson, A. 2004, ApJ, 613, 770
Maté, B., Tanarro, I., Escribano, R., Moreno, M., & Herrero, V. J. 2015, ApJ, 806, 151
Maté, B., Tanarro, I., Moreno, M. A., et al. 2014, Faraday Discuss, 168, 267
Mathis, J. S., Mezger, P. G., & Panagia, N. 1983, A&A, 128, 212
Mennella, V., Baratta, G. A., Esposito, A., Ferini, G., & Pendleton, Y. J. 2003, ApJ, 587, 727
Mennella, V., Brucato, J. R., Colangeli, L., & Palumbo, P. 1999, Astrophys J Lett, 524, L71
Mennella, V., Brucato, J. R., Colangeli, L., & Palumbo, P. 2002, ApJ, 569, 531
Mennella, V., Muñoz Caro, G. M., Ruiterkamp, R., et al. 2001, A&A, 367, 355
Moore, M. H., Hudson, R. L., & Gerakines, P. A. 2001, AcSpA, 57, 843
Pendleton, Y. J., & Allamandola, L. J. 2002, ApJ, 138, 75
Pendleton, Y. J., Sandford, S. A., Allamandola, L. J., Tielens, A. G. G. M., & Sellgren, K. 1994, ApJ, 473, 683
Pino, T., Dartois, E., Cao, A. T., et al. 2008, A&A, 490, 665
Prasad, S. S., & Tarafdar, S. P. 1983, ApJ, 267, 203
Roberge, W. G., Jones, D., Lepp, S., & Dalgarno, A. 1991, ApJS, 77, 287
Robertson, J. 1996, PhRvB, 53, 16302
Sandford, S. A., Allamandola, L. J., Tielens, A. G. G. M., et al. 1991, ApJ, 371, 607
Schnaiter, M., Henning, T., Mutschke, H., et al. 1999, ApJ, 519, 687
Schwarz-Selinger, T., Von Keudell, A., & Jacob, W. 1999, JAP, 86, 3988
Spitzer, L., Jr., & Tomashko, M. G. 1968, ApJ, 152, 971
Strazzulla, G., & Johnson, R. E. 1991, in Comets in the Post-Halley Era, ed. R. L. Newburn, M. Neugerbauer, & J. Rahe (Dordrecht: Kluwer), 243
Whittet, D. C. B., Boogert, A. C. A., Gerakines, P. A., et al. 1997, ApJ, 490, 729
Whittet, D. C. B., Gerakines, P. A., Hough, J. H., & Shenoy, S. S. 2001, ApJ, 547, 872
Wickramasinghe, D. T., & Allen, D. A. 1980, Natur, 287, 518
Ziegler, F. J., Ziegler, M. D., & Biersack, J. P. 2010, NIMPB, 268, 1818